Available online at www.sciencedirect.com
ScienceDirect
Computational Materials Science 41 (2008) 553–560
COMPUTATIONAL MATERIALS SCIENCE
www.elsevier.com/locate/commatsci

Molecular dynamics study of the mechanical behavior of nickel nanowire: Strain rate effects

Yu-Hua Wen [a,b], Zi-Zhong Zhu [a,*], Ru-Zeng Zhu [b]

[a] Department of Physics, and Institute of Theoretical Physics and Astrophysics, Xiamen University, Xiamen 361005, China
[b] LNM, Institute of Mechanics, Chinese Academy of Sciences, Beijing 100080, China

Received 15 December 2006; received in revised form 15 May 2007; accepted 24 May 2007
Available online 10 July 2007

Abstract

We present the analysis of uniaxial deformation of nickel nanowires using molecular dynamics simulations, and address the strain rate effects on mechanical responses and deformation behavior. The applied strain rate is ranging from 1×10^{8} s^{-1} to 1.4×10^{11} s^{-1}. The results show that two critical strain rates, i.e., 5×10^{9} s^{-1} and 8×10^{10} s^{-1}, are observed to play a pivotal role in switching between plastic deformation modes. At strain rate below 5×10^{9} s^{-1}, Ni nanowire maintains its crystalline structure with neck occurring at the end of loading, and the plastic deformation is characterized by {1 1 1} slippages associated with Shockley partial dislocations and rearrangements of atoms close to necking region. At strain rate above 8×10^{10} s^{-1}, Ni nanowire transforms from a fcc crystal into a completely amorphous state once beyond the yield point, and hereafter it deforms uniformly without obvious necking until the end of simulation. For strain rate between 5×10^{9} s^{-1} and 8×10^{10} s^{-1}, only part of the nanowire exhibits amorphous state after yielding while the other part remains crystalline state. Both the {1 1 1} slippages in ordered region and homogenous deformation in amorphous region contribute to the plastic deformation.

PACS: 61.46.+w; 62.20.Fe; 87.64.Aa

Keywords: Nanowire; Mechanical properties; Strain rate; Molecular dynamics

1. Introduction

In the past decade, nanometer-sized structures have attracted a great deal of interests due to its unique mechanical, electronic, optical, and magnetic properties, opening up a broad view of applications [1,2]. As one of the most important one-dimensional (1-D) nanostructures, metallic nanowires have been expected to play an important role in future electronic, optical and nanoelectromechanical devices. Metallic nanowires have been also employed as catalysis, superconductor, nanopipette probes, and reinforcing fibers in high-strength/light-weight composite materials, etc. [3–8].

Characterization of mechanical properties of nanowires is an increasingly important area of materials science, not only from scientific interests, but also from implications for constructing materials with specific mechanical properties. However, this work is a challenge to existing testing and measuring techniques because of the tiny dimension of a nanowire making the manipulation rather difficult [9,10]. In recent years, the mechanical deformation of nanowires have been studied by molecular dynamics simulations using either embodied-atom-method (EAM) [11–15] or effective-medium theory (EMT) [16] as well as first-principles method based on density functional theory (DFT) [17–20]. These studies focus on investigations of the structural transformation under uniaxial strain, stress–strain relationship, the conductance, and the correlation of the force (associated with the changes in the bonding of nanowires). Many studies have been dedicated to

* Corresponding author. Tel.: +86 592 2182248; fax: +86 592 2189426.
E-mail addresses: yhwen@xmu.edu.cn (Y.-H. Wen), zzhu@xmu.edu.cn (Z.-Z. Zhu).

0927-0256/$ - see front matter © 2007 Published by Elsevier B.V.
doi:10.1016/j.commatsci.2007.05.012

ascertaining the properties of gold nanowires, and show that the Au nanowires, before breaking under tensile stress, can get as thin as one-atom chains, and as long as five suspended atoms [17,20,21]. Nickel nanowires show superplastic behavior at lower strain rates, while at sufficiently high strain rates, it can transform continuously to an amorphous metal at constant temperature [12–14,22]. Recently, shape memory effect (SME) and pseudoelastic behavior are observed in Cu and Ag nanowires in molecular dynamics simulations [23–25]. Some works also investigate temperature, size and strain-rate effects on the axial elongation and transverse shear behavior of copper nanowires [26–29].

Because of the unique properties of metallic nanowires, they are important in next-generation structural materials, biosensors and future nanoscale devices. It is necessary to develop a quantitative understanding of the mechanical and structural properties of such metallic nanowires. Although much research had been done to quantify the mechanical behavior of metallic nanowires, few have been dedicated to the study of strain rate effects on the mechanical properties of metallic nanowires. In this paper, we will address these effects by using molecular dynamics calculations to simulate the uniaxial tensile mechanical deformation of metallic nanowire, and investigating the structural evolution of the mechanical deformation process. Details of the MD simulation are presented in the following section. We present a brief discussion of the MD results and comparison with other results in Section 3. The main conclusions are summarized in Section 4.

2. Potential model and simulation methods

In this work, MD simulations have been performed with the quantum corrected Sutten–Chen (Q-SC) type many-body force field modified by Kimura et al. [30] in which the parameters were optimized to describe the lattice parameter, cohesive energy, bulk modulus, elastic constants, phonon dispersion, vacancy formation energy, and surface energy, leading to an accurate description of many properties of metals and their alloys [31,32]. For the SC type force field, the total potential energy for a system of atoms can be written as

$$U = \sum_{i}^{N} U_i = \sum_{i}^{N} \lambda \left[\frac{1}{2} \sum_{j \neq i}^{N} V(R_{ij}) - c\sqrt{\rho_i} \right]. \quad (1)$$

Here $V(R_{ij})$ is a pair interaction function defined by the following equation:

$$V(R_{ij}) = \left(\frac{a}{R_{ij}} \right)^n, \quad (2)$$

accounting for the repulsion between the i and j atomic cores; ρ_i is a local electron density accounting for cohesion associated with atom i defined by

$$\rho_i = \sum_{j \neq i}^{N} \phi(R_{ij}) = \sum_{j \neq i}^{N} \left(\frac{a}{R_{ij}} \right)^m. \quad (3)$$

In Eqs. (1)–(3), R_{ij} is the distance between atoms i and j, a is a length parameter scaling all spacings (leading to dimensionless V and ρ); c is a dimensionless parameter scaling the attractive terms; λ sets the overall energy scale; n and m are integer parameters such that $n > m$. Given the exponents (n, m), c is determined by the equilibrium lattice parameter, and λ is determined by the total cohesive energy. The Q-SC potentials have already been used to study structural transitions between various phases of Ni, Cu and other face-centered-cubic (fcc) metals [13,26,33]. For the Q-SC type potential of Ni, the parameters are given as follows: $n = 10$, $m = 5$, $\lambda = 7.3767$ meV, $c = 84.745$, and $a = 3.5157$ Å.

The initial geometry of Ni nanowire is constructed from a large cubic fcc single crystal of nickel using certain cylindrical cutoff radii centered at a cubic interstitial site, in which the crystallographic orientations in the X-, Y- and Z-axis are taken to be in the directions of [1 0 0], [0 1 0], and [0 0 1], respectively. In the X and Y directions, the Ni nanowire spans a finite number of unit cells, while in the Z-direction an infinite wire was obtained by applying the periodic boundary condition. In the present paper, the diameter of the nanowire is 2.53 nm (~7.2 fcc unit cells), and the length of the nanowire as constructed is initially 24.61 nm (~70 fcc unit cells in z-direction), forming a 11 270-atom nickel nanowire. The wire was first thermally relaxed by running 50 000 steps with a time step of 1 fs in order to eliminate unfavorable configurations. During the relaxation process, the temperature is kept constant at 300 K based on Nose–Hoover thermostat [34], and the diameter and length of the nanowire are allowed to shrink (or expand) at zero press based on the Berendsen approach [35]. After relaxation, the diameter expands to ~2.592 nm, and the length contracts to ~24.035 nm. The contraction in axial direction and expansion in radial directions are attributed to surface relaxation phenomenon, in which lost symmetry of surface atoms results in surface tension under initial state. The nanowire contraction due to surface tension effect is determined by allowing the initial nanowire to relax to a zero stress state [29].

We have simulated the uniaxial deformation process of Ni nanowire, and emphasized the strain rate effects. The uniaxial tensile deformation of the nanowire is simulated at room temperature (300 K) and constant strain rate in which the length (in the Z-direction) of the nanowire is increased gradually. Different strain rates, from 1.0×10^8 s^{-1} to 1.4×10^{11} s^{-1}, are applied on the nanowire to study their effects on the deformation mechanism. It should be emphasized that the loading process of the tensile strain is different from those described in Refs. [12,13], where the tensile strain was applied with increment of 0.5% (or 0.4%) in its total length after some time steps. In the present work, the tensile strain in each time step along Z-direction is increased by $\Delta\varepsilon_z = \dot{\varepsilon}\Delta t$, where Δt is the time step, and $\dot{\varepsilon}$ the strain rate. During the deformation process, the temperature is kept constant based on Nose–Hoover chain dynamics [34], and the diameter of the nanowire is

allowed to shrink (or expand) in order to keep the transversal component of the stress (σ_{xx} and σ_{yy}) close to zero based on the Berendsen approach [35].

3. Results and discussion

In this section, we will present the simulation results and discuss them. As mentioned in the previous section, we calculate the average stress in the system as a function of the strain during the deformation, and so the stress–strain relationships can be obtained for the same system at different strain rate. In order to investigate the influence of strain rate, we deform the same sample using different strain rates in the range from $1\times10^{8}\ s^{-1}$ to $1.4\times10^{11}\ s^{-1}$. The strain rate adopted here is very high compared to that in experiment, because only very short period of time can be simulated due to the time scale of molecular dynamics set by the atomic motion. One consequence of the short time scale is that very high strain rates are required to get any reasonable deformation within the available time.

Fig. 1 illustrates the strain rate effects on the stress–strain curves. For all strain rates, the stress increases linearly with strain up to 11%. Below this value, the stress–strain curves are almost completely overlapped for all of strain rates applied, indicating that in the linear elastic region no plastic deformation occurs and the elastic properties of a nanowire is insensitive to strain rate. The Young's modulus is essentially independent of strain rate. According to the linear regression analysis of the stress–strain curves under the linear elastic region, we obtain the Young's modulus $E_{[0\,0\,1]}$ close to 70 GPa along the [0 0 1] direction at 300 K, which is only 35% of its bulk value ($E_{\text{bulk}} = 199.5$ GPa) [36]. This is partly due to the Q-SC potential applied in the present paper not exactly fitted to experimental elastic constant. For example, Kimura et al. [30] showed that the calculated elastic constant C_{11}, C_{12} and C_{44} from the fitted potential are 13.7%, −4% and 26% lower than those of experimental data, respectively. This result is also appreciably lower than that of the nanowire (about 90 GPa) calculated by Branicio et al. [12] due to different type of potential applied in simulations. Moreover, the extremely high surface-to-volume ratios of nanowires can affect the mechanical properties. Specifically, these surface atoms have fewer nearest neighbors and weaker bonding which lead to decreasing of Young's modulus along [1 0 0] direction. As a result, this value is close to 70% of the calculated $E_{[0\,0\,1]} = 101.7$ GPa [37] for Ni monocrystal in the same potential model.

Beyond the elastic region, the stress drops abruptly after the first yield point has been reached, while the plastic deformation appears. The strain rate displays a remarkable influence on the stress–strain behavior. For low strain rates, the stress–strain relations display a clear zig-zag curve as the strain is increased. The stress rises, and then drops in a repeating increase/decrease cycle, and the range of cycle is fluctuating, not a constant value. We can see many such cycles in stress–strain response before the stress gets to zero. The fracture occurs before 35% strain, and lower strain rate results in lower fracture strain. For high strain rates, the stress–strain relations display a very different behavior. We cannot see the distinct drops/raises cycle in stress as the strain increases. Instead, the stress decreases continuously, and the stress–strain curve becomes smooth. No fracture is observed below 60% strain. The difference of stress–strain curve indicates that what happened in tensile process are changing with the strain rate simulated.

The yield strength, as a much more important materials property, is a stress level related to the onset of irreversible plastic deformation, which is usually described by the yield stress σ_y, traditionally defined as the stress where the strain is 0.2% larger than what would be expected from extrapolation from the elastic region. Because the stress–strain behavior of nanowire is different from that of bulk materials, the yield stress is defined as the maximum value of stress in deformation process [38], and accordingly the strain value as the yield strain. The yield point can be seen

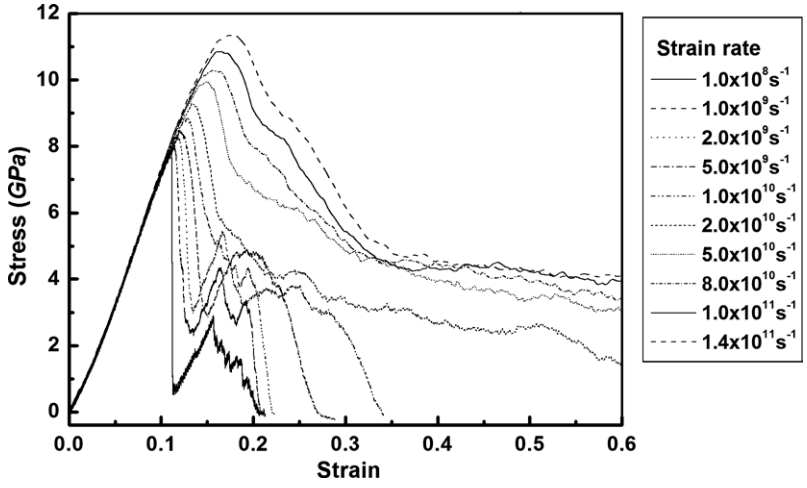

Fig. 1. The normal stress along Z-direction σ_{zz} as a function of the tensile strain for Ni nanowire at 300 K. The applied strain rates are from $1\times10^{8}\ s^{-1}$ to $1.4\times10^{11}\ s^{-1}$.

easily to be different with the strain rate applied from Fig. 1. We illustrate the dependence of the yield stress on the strain rate in Fig. 2. It seems that the yield stress rises up with the increasing of strain rate. We can divide stress–strain curves into three zones: below strain rate of $5\times10^{9}\,s^{-1}$, the strain rate dependence on the stress–strain curve is less pronounced; a strong dependence on the strain rate is seen for strain rate between $5\times10^{9}\,s^{-1}$ and $8\times10^{10}\,s^{-1}$; beyond strain rate of $8\times10^{10}\,s^{-1}$, the yield stress presents the strongest correlation with strain rate. So there are two "critical strain rate", i.e., $5\times10^{9}\,s^{-1}$ and $8\times10^{10}\,s^{-1}$, which are important for the study of deformation mechanism. The smallest yield stress of 7.98 GPa, obtained from the stress–strain curve, is far above that of experimental bulk Ni (about 0.14 GPa). When we compare the simulation results of yield stress with the experimental values, it is important to note that the experimental bulk samples have defects, such as dislocations, voids, and impurities, which favor the deformation process. The nanowire simulated in present paper, however, is defect-free and pure. The recent paper reports that the experimental value of the yield stress is 2.25 GPa for nanocrystalline Ni with a mean grain size of 26 nm [39]. This value, about one-third of the present simulated result, is reasonable considering that nanocrystalline Ni has a large fraction of grain boundaries and defects.

In MD simulations, we can obtain positions, velocities, and accelerations for all the atoms in the system at each time step. According to these data, the information of the structural evolution may be acquired through the common neighbor analysis (CNA) [40]. In this algorithm the bonds between an atom and its nearest neighbors are examined to determine the crystal structure. The CNA method has already been used successfully to analyse the structural evolution during the deformation and melting process [38,41–43]. In order to understand how and why the stress varies with the strain, we have studied the structure evolution of the tensile process under all of strain rates using CNA methods. We have calculated CNA indices for a number of atomic configurations extracted from the MD simulations. The different types of pairs are associated with different types of local order. All bonded pairs in the fcc crystal are of type 1421, while the hcp crystal has equal numbers of type 1421 and 1422. Considering that pairs beside types of 1421 and 1422 do not reveal some useful information for fcc metallic nanowire, here we have classified all atoms into three categories: 'fcc' atoms, having a local fcc order and considered to be inside the nanowire; 'hcp' atoms, having a local hcp order and classified as stacking faults; and 'other' atoms, all the other atoms considered as belonging to surface.

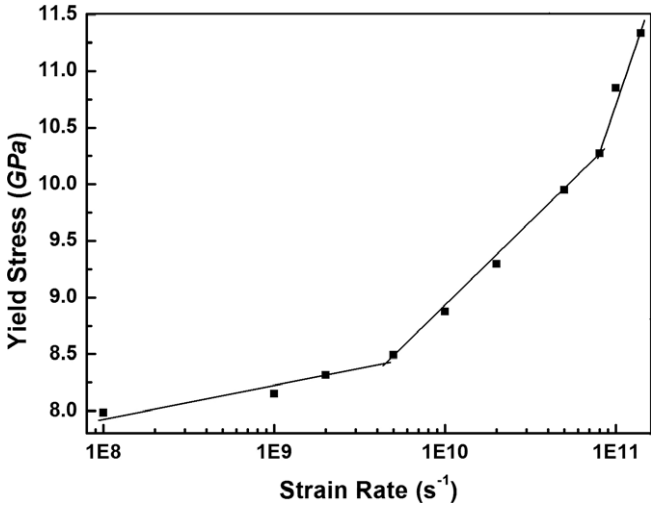

Fig. 2. Summary of the effect of varying the strain rate. The yield stress is seen to vary with the strain rate.

Fig. 3 presents the fraction of 'fcc' atoms and 'other' atoms as a function of tensile strain at all applied strain rates (the fraction of 'hcp' atoms can be deduced from this figure because all atoms beside these two types of atoms are 'hcp' atoms). For all strain rates, it can be seen that below 7.5 atoms keep at 65 which means that the structure has no change. When the strain is increased up to 11 strain rates. With the increasing strain, the number of 'fcc' atoms firstly drops, and then rise up. For different strain rates, the fluctuant trend and range are somewhat different. Below the strain rate of $5\times10^{9}\,s^{-1}$, the fraction of 'fcc' atoms changes in small range with the increasing strain, but the value stays above 50 large number of atoms belong to 'fcc' atoms, whereas the 'other' atoms are $401\times10^{10}\,s^{-1}$, the fraction of 'fcc' atoms abruptly decreases from 6535 above 45 the deformation process passing the yield point. Comparison between Fig. 3a and b, it shows that some of 'fcc' atoms change into 'other' atoms during the tensile process. The number of these 'fcc' atoms increases when the applied strain rate rises up. When the strain rate rises up to $8\times10^{10}\,s^{-1}$, the 'fcc' atoms are only 7 those atoms exceeding 81the structure is in serious disorder, and most of the system is in amorphous state. The 'fcc' atoms decreased further to 1.5 'other' atoms are up to 96.5 system changes completely into amorphous state.

To visualize the tensile process and explore the deformation mechanism, we draw some representative atomic configurations out from a large of data. For strain rate of $1\times10^{9}\,s^{-1}$, the nanowire has no 'hcp' atom until 11.4% strain. All 'fcc' atoms are distributed in the interior region, and all 'other' atoms are located in the surface layer, as shown in Fig. 4a. The nanowire substantially keeps its initial column shape. Beyond 11.4% strain, plastic deformation starts to take place in order to accommodate the applied strain. When the strain reaches 11.8%, a large number of 'hcp' atoms appear in the interior. The appearance of 'hcp' atoms in the system implies the formation of stacking faults caused by movement of Shockley partial dislocations, which can partially carry the plastic deformation by the slipping along $\langle 1\,1\,2\rangle$ directions in the $\{1\,1\,1\}$ planes. The preferential occurrence of $\{1\,1\,1\}$ slip planes is due to the smallest Burgers vector existing in the $\langle 1\,1\,0\rangle$ close-packed directions for fcc crystal structures, making

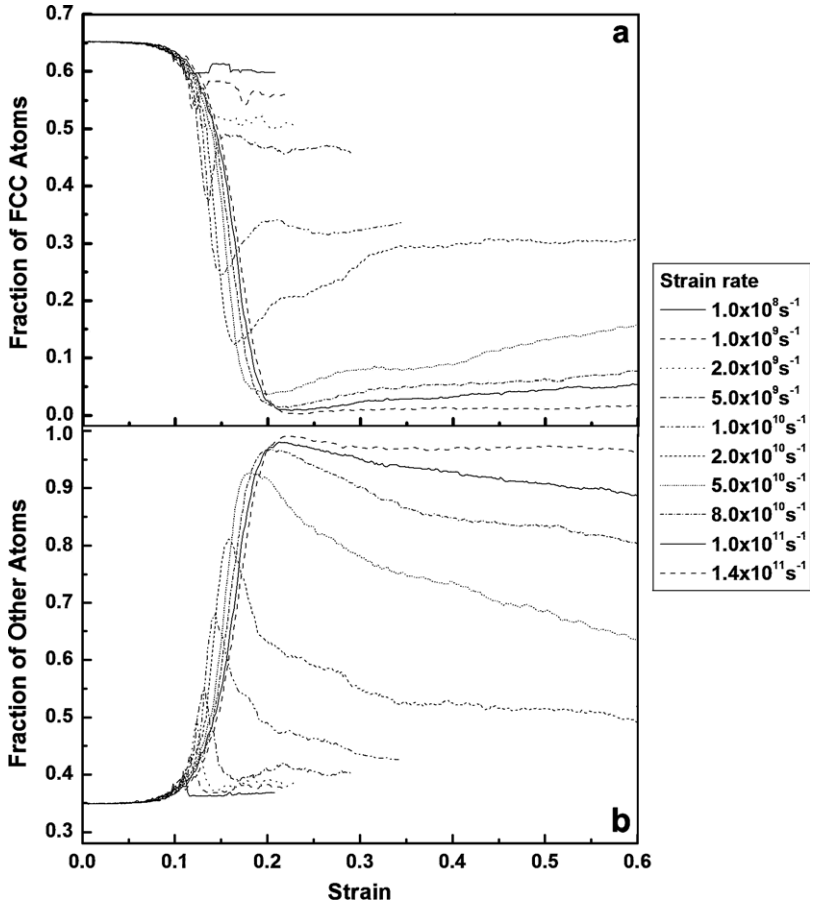

Fig. 3. CNA results for Ni nanowire. The fractions of two categories of atoms are shown as a function of the tensile strain at all applied strain rate. (a) The fraction of 'fcc' atoms. (b) The fraction of 'other' atoms.

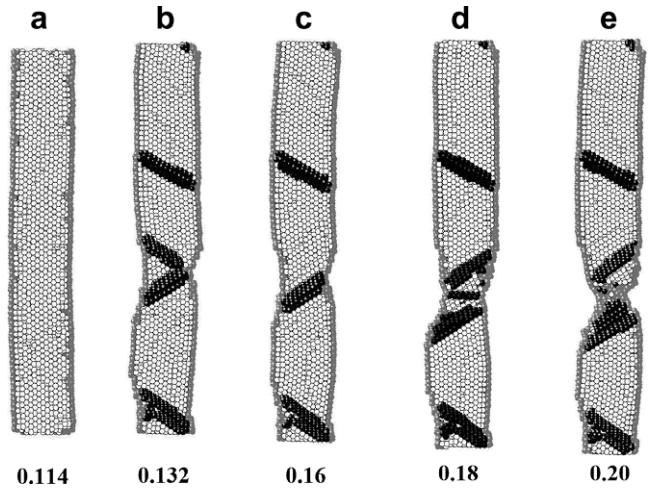

Fig. 4. The atomic configuration of Ni nanowire along X–Z section at several strain starting from a perfect fcc crystal at 300 K and the strain rate of $1\times10^{9}\ s^{-1}$. Atoms are color-coded according to the local crystalline order as determined by CNA: hollow atoms are in a fcc environment, black atoms are in a local hcp environment which are at stacking faults. Atoms in any other environment are colored gray which are typically at surface layers. The applied strains are: (a) 11.4%, (b) 13.2%, (c) 16%, (d) 18%, (e) 20%.

it most energetically favorable to reconstruct along this plane [11]. However, these partial dislocations first move in Ni nanowire because their activities need smaller energy than those of the dislocations with Burgers vector $\langle 1\,1\,0\rangle$. With the strain increasing, more slips occur along the $\{1\,1\,1\}$ planes. Fig. 4b displays the atomic configuration at the 13.2% strain. It is easily seen that there are mainly two $\{1\,1\,1\}$ planes playing a role in the present simulations, in spite of the $\{1\,1\,1\}$ planes including four different planes in the crystalline structure. This is because the forces driving the slipping of these two planes are smaller than other two planes. With the strain from 13.2% to 16%, the nanowire experiences again a series of slipping along $\langle 1\,1\,2\rangle$ directions, resulting in that stacking faults disappear, as shown clearly in Fig. 4c. During this process, necking starts to appear at the middle of the nanowire, the structure changes happen at the neck region, while other regions have no significant changes. With the strain increasing further more, we find that sliding along the $\{1\,1\,1\}$ planes happen (see Fig. 4d), and many atoms rearrange in the neck region. Beyond the strain of 18%, the fraction of 'hcp' atoms remains constant, no slippage appear during this process. Significant necking occurs after the strain of 20% (see Fig. 4e), and failure takes place at 21.2%. Through fur-

ther analysis, we find that after the formation of the neck, the plastic deformations have been carried mainly through the reconstruction and rearrangement of the neck region, which was previously reported in other studies [16,26]. Beyond this region, the nanowire keeps ordered structure and have no significant change.

As the strain rate is increased up to $2\times10^{10}\ s^{-1}$, the stress–strain curve of the nanowire displays "wavelets" after the first yield point (see Fig. 1). This indicates the presence of disorder in the nanowire, which is attributed to the onset of amorphous deformation of the nanowire at a high strain rate. This point can be seen from the result of CNA analysis, as shown in Fig. 3. Below the strain of 7.5%, the fraction of each category of atoms, and the structure has no significant change. With the strain increasing to 13%, about 10.7% of atoms with fcc crystal change into 'other' atoms. Some of 'other' atoms appear inside the system, but there is still no 'hcp' atoms, as illustrated in Fig. 5a. The 'hcp' atoms begin to occur at the strain of 13.2% and reach 18.8% at the strain of 19.2%. At this strain, some 'hcp' atoms arrange regularly in {1 1 1} plane, which is the result of slipping along ⟨1 1 2⟩ directions in this plane. This is somewhat similar to what happened for lower strain rates. But other 'hcp' atoms are scattered without regulation and do not form ordered structure in the system, meaning a local amorphous structure occur inside the nanowire. This disorder can be attributed to the influence of high strain rate. Due to insufficient strain rate, only a minor part of fcc crystal nanowire transform into amorphous (glasslike) state. When the strain is increased to 23%, the diameter of the nanowire along the axis shows a distinct non-uniform feature (see Fig. 5c). The necking can be seen at 30%, as displayed in Fig. 5d. Comparing this figure to Fig. 4d, we find that these are several necks at this strain rate. These necks can be seen more clearly when the strain is up to 50% (see Fig. 5e). If comparing the evolution of the deformation from Fig. 5b–e in detail, we can find that few slippages happened, whereas the amorphous region plays an important role in the deformation for strain greater than 19.2%. This is because the amorphous structure is mainly located in the necks, the stress in these regions is generally higher than that in other region, the plastic deformation can happen at this region easier than other region.

With the further increase of strain rate to $8\times10^{10}\ s^{-1}$, most atoms in the nanowire change to 'other' atoms (see Fig. 3), completely amorphous behaviors are observed at higher strain rate. As a respective example, we give several strains on the evolution of atomic configuration at $1\times10^{11}\ s^{-1}$ strain rate, as showed in Fig. 6. The yield point occurred at the strain of 16.5%, with corresponding yield stress of 10.85 GPa. This stress is up to 33.3% higher than that simulated at $1\times10^{9}\ s^{-1}$ strain rate. From Fig. 6a, we see that the structure remains to be a fcc crystal at 11% strain. With the strain increasing to 17% (beyond the yield strain), some 'other' atoms appear inside the system, and no 'hcp' atoms can be found. No {1 1 1} slip planes could be observed in this case, which are completely different from those presented in Figs. 4 and 5. At the strain of 26%, the transformation from fcc crystal to an amorphous state are accomplished completely, as illustrated in Fig. 6c. We can find some few 'hcp' and 'fcc' atoms scatter in the nanowire, but these atoms did not form certain ordered structure. Therefore the system is completely amorphous, which can be identified from the stress–strain relation as

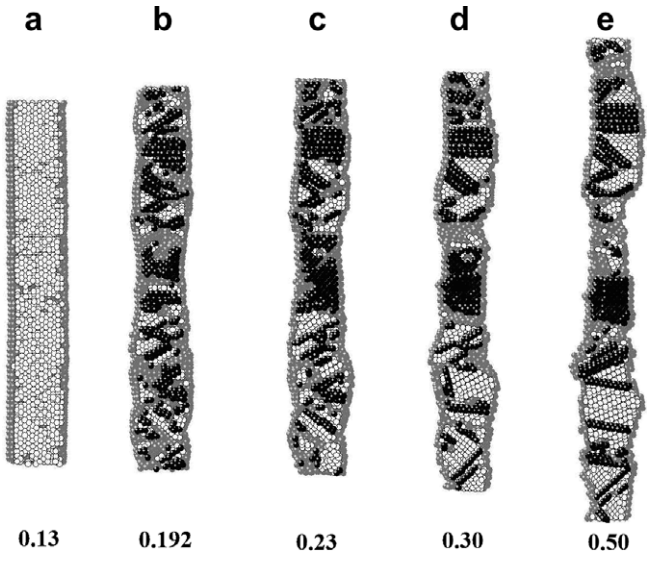

Fig. 5. The atomic configuration of Ni nanowire along X–Z section at several strain starting from a perfect fcc crystal at 300 K and the strain rate of $2\times10^{10}\ s^{-1}$. Atoms are color-coded as similar to Fig. 4 according to the local crystalline order as determined by CNA. The applied strains are: (a) 13%, (b) 19.2%, (c) 23%, (d) 30%, (e) 50%.

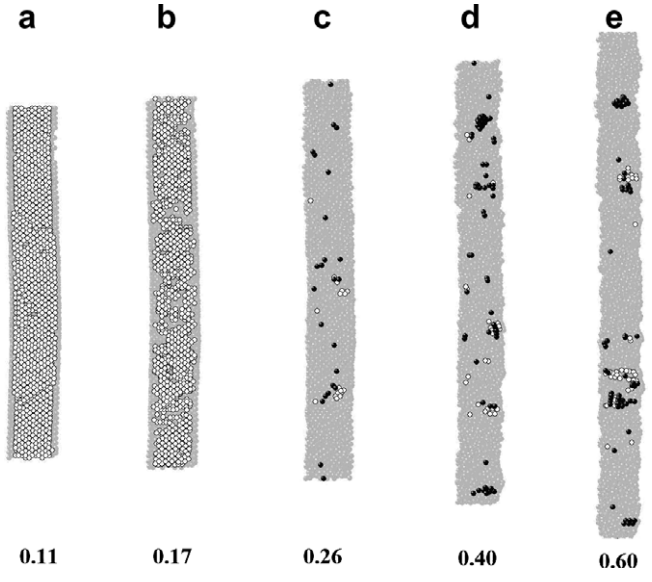

Fig. 6. The atomic configuration of Ni nanowire along X–Z section at several strain starting from a perfect fcc crystal at 300 K and the strain rate of $1\times10^{11}\ s^{-1}$. Atoms are color-coded as similar to Fig. 4 according to CNA methods. The applied strains are: (a) 11%, (b) 17%, (c) 26%, (d) 40%, (e) 60%.

shown in Fig. 1. This phenomenon is in good agreement with the observations of Ikeda et al. [13] for Ni and NiCu nanowires subjected to high strain rates. No dislocations are found during the tensile process of the nanowire. This is because higher strain rate induces higher dislocation speed in order to accommodate the plastic deformation. When the dislocation speed approaches the shear wave speed of nickel, the deformation mechanism can be transferred from {1 1 1} slippages through dislocation motion to amorphization [27]. The amorphous nanowire deformed uniformly, with no formation of necking until the end of simulation (see Fig. 6d and e). Superplastic behaviors arose in present simulation when the Ni nanowires are subjected to extremely high strain rate.

Finally, it may be pointed out that the strain rate adopted here is very high comparing to that in real experiment because only very short period of time can be simulated due to the time scale of molecular dynamics set by the atomic motion. So, it is unsuitable to directly compare the results under the strain rates adopted in this paper to that in real experiment. In spite of the short time scale, one may still obtain some reasonable results through molecular dynamics simulations within the available time for some phenomena of long time scales, such as the tensile deformation of nanotubes [44], phase transformations and grain nucleation [45], and diffusion process [46]. In addition, the critical strain rates are of vital importance in controlling the fabrication of metallic nanowire and its practical applications, and should rely on the diameter size and type of the nanowire. Further studies are undergoing and related results will be presented in our subsequent works.

4. Conclusion

In this paper, we have performed molecular dynamics simulations with the quantum Sutten–Chen many body force field to study the structural evolution and deformation behavior of nickel nanowire at different strain rates during the uniaxial tensile process. We addressed the strain rate effects on the deformation characteristics and mechanical properties of the nanowire. For all applied strain rates, the elastic deformation can reach about 11%, and at elastic stage the deformation happened mainly through the homogeneous elongation between the layers (perpendicular to the Z-axis) while the atomic structure remains essentially unchanged. We found two critical strain rates, i.e., $5\times10^{9}\ s^{-1}$ and $8\times10^{10}\ s^{-1}$, characterized in the deformation behavior. The influence of strain rate can be divided into three regions: (i) when the strain rate is below $5\times10^{9}\ s^{-1}$, the nanowire keeps its crystalline structure during the tensile process, the necking occurs in the last part of deformation. The deformation can be characterized by {1 1 1} slippages associated with Shockley partial dislocations and rearrangements of atoms close to necking regions. (ii) When the strain rate is between $5\times10^{9}\ s^{-1}$ and $8\times10^{10}\ s^{-1}$, part of nanowire transforms from a fcc crystal to amorphous state, and the other part still keeps its ordered structure during the tensile process. Several necks can be observed after certain strain. The {1 1 1} slippages in the ordered region and rearrangements of atoms including the amorphous region are offered to the plastic deformation of nanowire. (iii) When the strain rate is above $8\times10^{10}\ s^{-1}$, the nanowire completely transforms into amorphous state during the deformation process beyond the elastic limit. The nanowire deformed uniformly without dislocation activities and formation of obvious necking until the end of simulation.

Acknowledgements

Financial support is provided by the National 973 Project of China (No. 2006CB605102), and the Program for New Century Excellent Talents in Fujian Province University (NCETFJ). In addition, Y.H. Wen acknowledges support from the State Key Laboratory of Nonlinear Mechanics (LNM), Chinese Academy of Science. The authors also thank beneficial discussions with Dr. H. Liang and Dr. H. Fang.

References

[1] H. Gleiter, Prog. Mater. Sci. 33 (1989) 223.
[2] H. Gleiter, Acta Mater. 48 (2000) 1.
[3] Y. Kondo, K. Takayanagi, Science 289 (2000) 606.
[4] B.A. Glavin, Phys. Rev. Lett. 86 (2001) 4318.
[5] S. Iijima, L.C. Qin, Science 296 (2002) 611.
[6] A. Bietscha, B. Michel, Appl. Phys. Lett. 80 (2002) 3346.
[7] M. Kawamura, N. Paul, V. Cherepanov, B. Voigtländer, Phys. Rev. Lett. 91 (2003) 096102.
[8] N.A. Melosh et al., Science 300 (2003) 112.
[9] Z.L. Wang et al., Adv. Eng. Mater. 3 (2001) 657.
[10] D. Erts, H. Olin, J.D. Holmes, Proc. SPIE 5123 (2003) 248.
[11] G.M. Finbow, R.M. Lynden-Bell, I.R. McDonald, Mol. Phys. 92 (1997) 705.
[12] P.S. Branicio, J.P. Rino, Phys. Rev. B 62 (2000) 16950.
[13] H. Ikeda, Y. Qi, T. Cagin, K. Samwer, W.L. Johnson, W.A. Goddard, Phys. Rev. Lett. 82 (1999) 2900.
[14] U. Landman, W.D. Luedtke, B.E. Salisbury, R.L. Whetten, Phys. Rev. Lett. 77 (1996) 1362.
[15] H. Liang, M. Upmanyu, H. Huang, Phys. Rev. B 71 (2005) 241403.
[16] M.R. Sorensen, M. Brandbyge, K.W. Jacobsen, Phys. Rev. B 57 (1998) 3283.
[17] E.Z.D. Silva, A.J.R.D. Silva, A. Fazzio, Phys. Rev. Lett. 87 (2001) 256102.
[18] P. Jelınek, R. Perez, J. Ortega, F. Flores, Phys. Rev. B 68 (2003) 085403.
[19] A. Nakamura, M. Brandbyge, L.B. Hansen, K.W. Jacobsen, Phys. Rev. Lett. 82 (1999) 1538.
[20] E.Z. da Silva, F.D. Novaes, A.J.R. da Silva, A. Fazzio, Phys. Rev. B 69 (2004) 115411.
[21] R.N. Barnett, U. Landman, Nature 387 (1997) 788.
[22] P. Walsh, W. Li, R.K. Kalia, A. Nakano, P. Vashishta, S. Saini, Appl. Phys. Lett. 78 (2001) 3328.
[23] W. Liang, M. Zhou, F. Ke, Nano Lett. 5 (2005) 2039.
[24] H.S. Park, K. Gall, J.A. Zimmerman, Phys. Rev. Lett. 95 (2005) 255504.
[25] H.S. Park, C. Ji, Acta Mater. 54 (2006) 2645.
[26] S.J.A. Koh, H.P. Lee, C. Lu, Q.H. Cheng, Phys. Rev. B 72 (2005) 085414.
[27] W. Liang, M. Zhou, Struct. Dyn. Mater. Conf. 3 (2004) 2057.

[28] W. Liang, M. Zhou, J. Mech. Eng. Sci. 218 (2004) 599.
[29] S.J.A. Koh, H.P. Lee, Nanotechnology 17 (2006) 3451.
[30] Y. Kimura, Y. Qi, T. Cagin, W.A. Goddard, unpublished.
[31] Y. Qi, T. Cagin, W.L. Johnson, W.A. Goddard, J. Chem. Phys. 115 (2001) 385.
[32] Y. Qi, Y.T. Cheng, T. Cagin, W.A. Goddard, Phys. Rev. B 66 (2002) 085420.
[33] Y.H. Wen, Z.Z. Zhu, G.F. Shao, R.Z. Zhu, Physica E 27 (2005) 113.
[34] D.J. Evans, B.L. Holian, J. Chem. Phys. 83 (1985) 4069.
[35] H.J.C. Berendsen, J.P.M. Postma, W.F. van Gunsteren, J. Chem. Phys. 81 (1984) 3684.
[36] R.W. Hertzberg, Deformation and Fracture Mechanics of Engineering Materials, Wiley, New York, 1983.
[37] Y.H. Wen, S.Q. Wu, Z.Z. Zhu, unpublished.
[38] J. Schiotz, F.D.D. Tolla, K.W. Jacobsen, Nature 391 (1998) 561.
[39] Z. Budrovic, H.V. Swygenhoven, P.M. Derlet, S.V. Petegem, B. Schmitt, Science 304 (2004) 273.
[40] J.D. Honeycutt, H.C. Andersen, J. Phys. Chem. 91 (1987) 4950.
[41] J. Schiotz, K.W. Jacobsen, Science 301 (2003) 1357.
[42] H.V. Swygenhoven, Science 296 (2002) 66.
[43] V. Yamakov, D. Wolf, S.R. Phillpot, A.K. Mukherjee, Nature Mater. 1 (2002) 1.
[44] Y.R. Jeng, P.C. Tsai, T.H. Fang, Phys. Rev. B 71 (2005) 085411.
[45] A. Latapie, D. Farkas, Model. Simul. Mater. Sci. Eng. 11 (2003) 745.
[46] E. Beerdsen, B. Smit, D. Dubbeldam, Phys. Rev. Lett. 93 (2004) 248301.